A Conservative Lattice Boltzmann Model for the Volume-Averaged Navier-Stokes Equations Based on a Novel Collision Operator

Bruno Blais[a], Jean-Michel Tucny[a], David Vidal[a], François Bertrand[a,*]

[a] *Research Unit for Industrial Flow Processes (URPEI), Department of Chemical Engineering, École Polytechnique de Montréal, P.O. Box 6079, Stn Centre-Ville, Montréal,QC, Canada, H3C 3A7*

Abstract

The volume-averaged Navier-Stokes (VANS) equations are at the basis of numerous models used to investigate flows in porous media or systems containing multiple phases, one of which is made of solid particles. Although they are traditionally solved using the finite volume, finite difference or finite element method, the lattice Boltzmann method is an interesting alternative solver for these equations since it is explicit and highly parallelizable. In this work, we first show that the most common implementation of the VANS equations in the LBM, based on a redefined collision operator, is not valid in the case of spatially varying void fractions. This is illustrated through five test cases designed using the so-called method of manufactured solutions. We then present a LBM scheme for these equations based on a novel collision operator. Using the Chapman-

*Corresponding author
Email address: francois.bertrand@polymtl.ca (François Bertrand)

Enskog expansion and the same five test cases, we show that this scheme is second-order accurate, explicit and stable for large void fraction gradients.
Keywords: Computational fluid dynamics; Volume-averaged Navier-Stokes equations; Lattice Boltzmann method; Method of manufactured solutions; Multiphase flows; Porous media.

1. Introduction

Multiphase flows play a critical role in numerous key unit operations in the process industry such as mixing [1], transport [2] and fluidization [3]. Due to their complexity, they are often the bottleneck in the design and the operation of these units. Although the experimental study of these systems has led to a better understanding of their behavior, numerical simulation has proved an efficient and complementary tool to gain a deeper knowledge of the underlying flows.

Due to the steady increase of computational power, the last decades have witnessed the development of numerous numerical models that are capable of resolving multiphase flows with various length and time scales [4]. Among these, the two-fluid model [5, 6], the combination of classical CFD approaches and the discrete element method (DEM) dubbed CFD-DEM [7], and the multiphase particle-in-cell (MP-PIC) method [8] have been used extensively to study, in

particular, solid-fluid flows such as those in solid-liquid mixing [9], fluidized beds and pneumatic transport [3]. In such cases, these methods all have in common that they are based on the solution of a volume-averaged form of the Navier-Stokes (VANS) equations for either the two phases (two-fluid model) or for the fluid only (CFD-DEM and MP-PIC). The VANS equations have also been used extensively in the study of porous media, in which the porosity is a function of space [10].

Traditionally, the VANS equations have been solved using classical numerical methods such as the finite volume method [11, 12, 13, 14], the finite difference method [15] or the finite element method [10]. However, alternative numerical approaches have been proposed in recent years in the hope of increasing the versatility and the computational speed of the standard methods. These models are based on the use of smoothed particle dynamics (SPH) [16] or the lattice Boltzmann method (LBM) [17, 18, 19, 20].

Between the last two numerical paradigms, the lattice Boltzmann method is an appealing candidate for the solution of the VANS equations. Indeed, this method is explicit and highly parallelizable, making it the ideal fluid solver in models such as CFD-DEM, which is generally computationally intensive because it requires small CFD time steps to ensure the stability of the coupling

between the two phases. However, the solution of the VANS equations using the LBM requires a modified scheme to take into account the void fraction. The schemes that have been proposed in the literature can be grouped into two main categories. The first kind is based on a reformulation of the collision operator and an additional term to recover a pressure gradient that is independent of the void fraction [18, 19, 20]. In the present work, this type of model is referred to as pressure-correction LBM-VANS scheme. The second kind is based on a non-conservative formulation of the VANS equations, and uses the classical LBM scheme along with mass and momentum source terms to recover the VANS equations [17].

As will be demonstrated in this paper, the pressure correction schemes are generally inadequate, even in the case of small void fraction gradients, due to their lack of robustness and accuracy. On the other hand, the non-conservative schemes require the use of mass source terms for which the implementation in the LBM is much more complex, requiring the solution of matrix systems and local sub-iterations. Furthermore, the expected second-order convergence of these two types of schemes has not been verified for non-trivial test cases in which the velocity and the volume fraction vary in space. This can be explained, at least in part, by the lack of non-trivial analytical solutions for the VANS equations.

Recently, Blais and Bertrand [21] have shown that the method of manufactured solutions (MMS) can be used to design complex test cases for the VANS equations, for which the convergence analysis of a solver can be carried out. They applied it successfully for the verification of the VANS equations within the CFDEM framework [22], which is based on the finite volume library Open∇FOAM [23] and DEM code LIGGGHTS [24, 25].

In this work, we briefly present the VANS equations and recall the pressure-correction LBM-VANS scheme that has been proposed in the literature. Then, we explain how the method of manufactured solutions can be used to design analytical solutions for these equations. We show by means of five test cases that this pressure-correction LBM-VANS scheme suffers from instabilities, notably in situations where the fluid is static (no-flow tests). We then introduce a new LBM-VANS scheme that relies on a new collision operator originating from the so-called immiscible multiphase lattice Boltzmann method [26]. This model is analyzed theoretically using a Chapman-Enskog expansion before it is verified using the same five test cases. We show that this new LBM-based model is second-order accurate and discuss its robustness.

2. Volume-Averaged Navier-Stokes Equations

A number of forms of the VANS equations have been proposed in the literature for multiphase flows. The main differences between these forms relate to the treatment of the interphase coupling and the expression for the stress tensor, as thoroughly discussed by Zhou *et al.* [11] for the two-fluid and the CFD-DEM models.

In this work, we consider without loss of generality the so-called form A of the VANS equations, which is based on local averaging. We refer to the book by Gidaspow [6] for an in-depth description of the origin of the model. The form A of the VANS equations will be simply referred to as the VANS equations in the remainder of this work.

The incompressible VANS equations are:

$$\frac{\partial \epsilon_f}{\partial t} + \nabla \cdot (\epsilon_f \boldsymbol{u}) = 0 \tag{1}$$

$$\frac{\partial (\rho_f \epsilon_f \boldsymbol{u})}{\partial t} + \nabla \cdot (\rho_f \epsilon_f \boldsymbol{u} \otimes \boldsymbol{u}) = -\epsilon_f \nabla p + \nabla \cdot \boldsymbol{\tau} + \boldsymbol{F} \tag{2}$$

where ϵ_f is the void fraction, ρ_f the density of the fluid, p the pressure, $\boldsymbol{u}$ the velocity and $\boldsymbol{F}$ a momentum source term. The viscous stress tensor, $\boldsymbol{\tau}$, is

defined as [7]:

$$\boldsymbol{\tau} = \mu\epsilon_f \left((\nabla \boldsymbol{u}) + (\nabla \boldsymbol{u})^T - \frac{2}{3} (\nabla \cdot \boldsymbol{u}) \boldsymbol{\delta}_k \right) \tag{3}$$

where μ is the dynamic viscosity and $\boldsymbol{\delta}_k$ the identity tensor.

It is important to note that the velocity and void fraction resulting from these equations are not individually divergence free, which means that all terms of the stress tensor are *a priori* non-zero.

3. Lattice Boltzmann Method

The Lattice Boltzmann Method (LBM) is based on the kinetic theory of gas and comes from the discretization in space, velocity and time of the Boltzmann equation. In fact, the LBM may be interpreted as the projection of the velocity space of the Boltzmann equation onto an isotropic orthonormal Hermite polynomial basis [27]. Consequently, the lattice Boltzmann method does not solve the incompressible Navier-Stokes equations *per se*, but a weakly compressible and athermal form of these equations which tend towards their incompressible form in the limit of low Mach number [28]. In the present work, only a brief presentation of the LBM is given. We refer the reader to the books by Succi [28] and Guo [29] for more details.

In the LBM, the primitive variable $f_i(\boldsymbol{x}, t)$ is mesoscopic and describes the ith a population (probability density function) of particles at position $\boldsymbol{x}$ and time t, with discrete velocity $\boldsymbol{\xi}_i$. Using the Bhatnagar-Gross-Krook (BGK) approximation [30], the particle population collision process is governed by the following lattice Boltzmann equation (LBE):

$$f_i\left(\boldsymbol{x}+\boldsymbol{\xi}_i\Delta t, t+\Delta t\right) - f_i\left(\boldsymbol{x}, t\right) = \frac{1}{\bar{\tau}}\left(f_i^{eq}\left(\boldsymbol{x}, t\right) - f_i\left(\boldsymbol{x}, t\right)\right) + \Delta t \boldsymbol{G}_i \tag{4}$$

with Δx the lattice spacing, $\bar{\tau}$ the dimensionless relaxation time, $\boldsymbol{G}_i$ a forcing term, Δt the time step, the term f_i^{eq} is the equilibrium distribution function:

$$f_i^{eq} = w_i \rho_f \left(1 + \frac{\left(\boldsymbol{\xi}_i \cdot \boldsymbol{u}\right)}{c_s^2} + \frac{\left(\boldsymbol{\xi}_i \cdot \boldsymbol{u}\right)^2}{2c_s^4} - \frac{\boldsymbol{u}\cdot\boldsymbol{u}}{2c_s^2}\right) \tag{5}$$

where c_s is the lattice speed of sound (celerity) defined as:

$$c_s = \frac{1}{\sqrt{3}}\frac{\Delta x}{\Delta t} \tag{6}$$

Furthermore, the forcing term $\boldsymbol{G}_i$ in the lattice Boltzmann equation is the form proposed by Guo [29]:

$$\boldsymbol{G}_i = \left(1 - \frac{1}{2\bar{\tau}}\right) w_i \left(\frac{\left(\boldsymbol{\xi}_i - \boldsymbol{u}\right)}{c_s^2} + \frac{\left(\boldsymbol{\xi}_i \cdot \boldsymbol{u}\right)}{c_s^4}\boldsymbol{\xi}_i\right) \cdot \boldsymbol{F} \tag{7}$$

where w_i is the discrete weight associated with discrete velocity $\boldsymbol{\xi}_i$.

Finally, the dimensionless relaxation time $\bar{\tau}$ can be related to the dynamic viscosity of the fluid μ via the lattice spacing Δx, the time step Δt and the

density of the fluid ρ_f, using the following relation :

$$\bar{\tau} = \frac{\mu}{\rho_f c_s^2 \Delta t} + \frac{1}{2} \tag{8}$$

In the present work, we solve the LBE in 2D using the well-established D2Q9 lattice stencil, which uses 9 discrete velocities [31]. More explicitly, the discrete velocities and weights are given by :

$$\boldsymbol{\xi}_i = \begin{cases} (0,0) & \text{for } i = 0 \\ \left(cos[\pi \frac{(i-1)}{2}], sin[\pi \frac{(i-1)}{2}]\right) \frac{\Delta x}{\Delta t} & \text{for } i \in [1,4] \\ \left(cos[\pi \frac{(i-\frac{9}{2})}{2}], sin[\pi \frac{(i-\frac{9}{2})}{2}]\right) \sqrt{2} \frac{\Delta x}{\Delta t} & \text{for } i \in [5,8] \end{cases} \tag{9}$$

$$w_i = \begin{cases} \frac{4}{9} & \text{for } i = 0 \\ \frac{1}{9} & \text{for } i \in [1,4] \\ \frac{1}{36} & \text{for } i \in [5,8] \end{cases} \tag{10}$$

From a computational point of view, the LBE is solved using a two-step process. First, a collision step is done, followed by a propagation step. These two steps can be written respectively as :

$$f_i\left(\boldsymbol{x}, t^+\right) = f_i\left(\boldsymbol{x}, t\right) - \frac{1}{\bar{\tau}}\left(f_i\left(\boldsymbol{x}, t\right) - f_i^{eq}\left(\boldsymbol{x}, t\right)\right) + \Delta t \boldsymbol{G}_i \tag{11}$$

$$f_i\left(\boldsymbol{x} + \boldsymbol{\xi}_i \Delta t, t + \Delta t\right) = f_i\left(\boldsymbol{x}, t^+\right) \tag{12}$$

This LBM scheme has been implemented in the *vansBurst* LBM code, which is a 2D serial C++ code designed by our group for an easy integration of alternative collision operators.

4. Pressure-correction LBM-VANS scheme

The lattice Boltzmann method is intrinsically linked to the Navier-Stokes equations. Consequently, it requires modifications before it can be used to solve the volume-averaged Navier-Stokes equations. One method to obtain the VANS equations in the context of the LBM, as has been proposed by [18, 19, 20], is based on a rescaling of the density in the equilibrium distribution function by the void fraction. Using this approach, one obtains the following expression for the populations at equilibrium :

$$f_i^{eq} = w_i \rho_f \epsilon_f \left(1 + \frac{(\boldsymbol{\xi}_i \cdot \boldsymbol{u})}{c_s^2} + \frac{(\boldsymbol{\xi}_i \cdot \boldsymbol{u})^2}{2c_s^4} - \frac{\boldsymbol{u} \cdot \boldsymbol{u}}{2c_s^2} \right) \tag{13}$$

Using this expression, the following equations are recovered in the low Mach number limit [20]:

$$\frac{\partial \rho_f \epsilon_f}{\partial t} + \nabla \cdot (\rho_f \epsilon_f \boldsymbol{u}) = 0 \tag{14}$$

$$\frac{\partial (\rho_f \epsilon_f \boldsymbol{u})}{\partial t} + \nabla \cdot (\rho_f \epsilon_f \boldsymbol{u} \otimes \boldsymbol{u}) = -\nabla (p \epsilon_f) + \nabla \cdot \boldsymbol{\tau} + \boldsymbol{F} \tag{15}$$

As can be seen, the pressure term resulting from this rescaling does not correspond to the one in Eq. (2) of the VANS equations. Therefore, the pressure must be corrected by adding $\boldsymbol{F}^P(\boldsymbol{x},t) = p\nabla\epsilon_f$ to $\boldsymbol{F}(\boldsymbol{x},t)$ in (7), which gives:

$$\boldsymbol{G}_i = \left(1 - \frac{1}{2\bar{\tau}}\right) w_i \left(\frac{(\boldsymbol{\xi}_i - \boldsymbol{u})}{c_s^2} + \frac{(\boldsymbol{\xi}_i \cdot \boldsymbol{u})}{c_s^4}\boldsymbol{\xi}_i\right) \cdot \left(\boldsymbol{F} + \boldsymbol{F}^P\right) \tag{16}$$

This additional source term must be enforced separately using for instance the method proposed by Guo [29]. In our implementation of this scheme, this gradient is calculated using a second-order centered finite difference scheme. This scheme is referred to as the pressure correction LBM-VANS scheme. In theory, it allows to recover the VANS equations. However, the pressure in the LBM is defined using an equation of state that depends on ρ_f:

$$p = \rho_f c_s^2 \tag{17}$$

Assuming that ϵ_f is sufficiently smooth, refining the grid should lead to a converged expression for both ρ_f and $\nabla\epsilon_f$. However, Eqs. (6) and (8) show that, for a constant relaxation time $\bar{\tau}$, c_s^2 increases to infinity asymptotically as the mesh is refined. This scheme is thus expected to be ill-behaved in the limit $\Delta x \to 0$, which prevents it from converging consistently to the VANS equations. To our knowledge, the present work is the first time that a thorough convergence study is done for this scheme using test cases that involve non constant void fractions.

5. Method of Manufactured Solutions

The method of manufactured solutions (MMS) is a generic approach that allows one to build analytical solutions to partial differential equations (PDE) [32]. Its particular strength is that it allows to choose *a priori* a solution to a PDE with given properties (e.g., infinite differentiability or local integrability). Such a solution can then be used to verify rigorously and in a flexible manner the implementation of any given solver.

The MMS procedure is straightforward. In the case of the VANS equations for a single fluid, we choose a velocity field $\boldsymbol{u}$ and a void fraction ϵ_f, and build a vector of manufactured variables $\boldsymbol{s}_{\mathrm{M}} = [\boldsymbol{u}^T, \epsilon_f]^T$ that satisfies the continuity equation (1).

In general, $\boldsymbol{s}_{\mathrm{M}}$ is not a solution of the complete VANS equations because it does not satisfy the momentum conservation equation (2). To do so, the following momentum source term $\boldsymbol{H}$ is added to this momentum conservation equation:

$$\begin{aligned}\boldsymbol{H}(\boldsymbol{s}_M) =& \frac{\partial\left(\rho_f \epsilon_f \boldsymbol{u}\right)}{\partial t} + \nabla \cdot \left(\rho_f \epsilon_f \boldsymbol{u} \otimes \boldsymbol{u}\right) + \epsilon_f \nabla p \\ & - \nabla \cdot \left(\mu \epsilon_f \left(\left(\nabla \boldsymbol{u}\right) + \left(\nabla \boldsymbol{u}\right)^T - \frac{2}{3}\left(\nabla \cdot \boldsymbol{u}\right)\boldsymbol{\delta}_k \right)\right) \end{aligned} \tag{18}$$

With this definition of $\boldsymbol{H}$, the manufactured solution is an analytical solution

of the VANS equations (1) and (2).

This solution can be used to assess the accuracy of the pressure-correction LBM-VANS scheme (or any other scheme) by monitoring the decrease of the Euclidean norm of the error ($\|e\|_2$) with respect to the lattice spacing (Δx). As the LBM uses a Cartesian, homogenous and regular structured grid, this error is defined as:

$$\|e_{\boldsymbol{\chi}}\|_2 = \sqrt{\frac{1}{N}\sum_{j}^{N} \|\boldsymbol{\chi}_{M,j} - \boldsymbol{\chi}_j\|^2} \tag{19}$$

where N is the number of lattices, $\boldsymbol{\chi}_{M,j}$ the manufactured (or analytical) solution at cell j, and $\boldsymbol{\chi}_j$ the numerical solution at the same position. The order of convergence obtained via simulations can be compared with the theoretical second order of convergence of the LBM scheme. Another type of error that will be monitored in some of the test cases described in the next section is the infinity norm, which is defined as:

$$\|e_{\boldsymbol{\chi}}\|_\infty = \max_j \|\boldsymbol{\chi}_{\mathrm{M},j} - \boldsymbol{\chi}_j\| \tag{20}$$

In the present work, analytical expressions for the source terms $\boldsymbol{H}(x, y)$ were obtained symbolically through Eq. (18) calculated using Mathematica 8 [33]. These expressions were translated to C++ syntax and directly integrated in our *vansBurst* LBM code using the CForm command of Mathematica.

6. Methodology

In this section, we present five test cases of increasing complexity that we used to assess the validity of the LBM-VANS schemes. For all these test cases, the simulations were carried out for numerous lattice grids on the two-dimensional domain $\Omega = [-1, 1] \times [-1, 1]$. Periodic boundary conditions were used in order to preclude the possible effect on accuracy of the method of, for instance, the technique considered for the imposition of non-zero Dirichlet boundary conditions. For the convergence analysis, grids comprised from 400 to 160000 lattice cells. The relaxation time $\bar{\tau}$ was set to 1 for each simulation, resulting in a diffusive scaling for the time step and an asymptotically vanishing Mach number.

6.1. Case 1: constant void fraction

The first manufactured case is defined as:

$$\boldsymbol{u} = 2 \begin{bmatrix} -\left(\sin\left(\pi x\right)\right)^2 \sin\left(\pi y\right) \cos\left(\pi y\right) \\ \\ \sin\left(\pi x\right) \cos\left(\pi x\right) \left(\sin\left(\pi y\right)\right)^2 \end{bmatrix} \tag{21}$$

$$\epsilon_f = \frac{3}{4} \tag{22}$$

where x and y are the coordinates in the Cartesian frame of reference.

This test case is rather simplistic as the void fraction ϵ_f is constant and the pressure correction term in Eq. (16) is zero. While it does not represent a comprehensive test for the VANS equations, it serves to verify the implementation of the LBM schemes in our code.

6.2. Case 2: no-flow with continuous void fraction

The second test case consists of what is referred to as a no-flow test, which means that the velocity is static: $\boldsymbol{u} = [0,\ 0]^T$. However, the void fraction is a continuous field:

$$\epsilon_f = \frac{3}{4} + \frac{1}{4}\sin(\pi x)\sin(\pi y) \tag{23}$$

The interest of this test, for which the momentum source term $\boldsymbol{H} = 0$ in Eq. (18), comes from the fact that it can serve to assess the stability of a scheme in the presence of void fraction gradients in the domain. In this case, the velocity should remain zero as there is no driving force for the flow.

6.3. Case 3: no-flow with discontinuous void fraction

The third test case is also a no-flow test. It involves the following discontinuous void fraction:

$$\epsilon_f = \begin{cases} 0.75, \ \ \forall \ \ (x,y) \in \Omega_s = [-0.04, 0.04] \times [-0.04, 0.04] \\ \\ 1, \ \ \forall \ \ (x,y) \in \Omega \backslash \Omega_s \end{cases} \tag{24}$$

It is similar to a two-dimensional step function. Such discontinuous functions are often encountered as an initial condition in real applications. For example, a bed of particles at the bottom of a vessel can be associated with a one-dimensional step function.

6.4. Case 4: steady-state divergence-free flow

The fourth case is defined as:

$$\boldsymbol{u} = 2 \begin{bmatrix} -\left(\sin\left(\pi x\right)\right)^2 \sin\left(\pi y\right) \cos\left(\pi y\right) \\ \\ \sin\left(\pi x\right) \cos\left(\pi x\right) \left(\sin\left(\pi y\right)\right)^2 \end{bmatrix} \tag{25}$$

$$\epsilon_f = \frac{3}{4} + \frac{1}{4} \sin\left(\pi x\right) \sin\left(\pi y\right) \tag{26}$$

This case is different from Case 1 since the void fraction is now a function of space.

6.5. Case 5: steady-state non divergence-free flow

The fifth case is defined as:

$$\boldsymbol{u} = Ae^{K\sin(\pi x)\sin(\pi y)}\,[1,\ 1]^T \tag{27}$$

$$\epsilon = Be^{-K\sin(\pi x)\sin(\pi y)} \tag{28}$$

where A, B, K are constants whose values are respectively 0.5, 0.7 and 0.3. This test case is the most complete of the five cases as the velocity field is non-divergence free and the void fraction varies in space. Therefore, all the terms of the viscous stress tensor (Eq. (3)) are non-zero.

7. Results and discussion on the pressure-correction LBM-VANS scheme

The graph in Figure 1 shows that, for Case 1, the velocity exhibits second-order convergence. However, as previously mentioned, this test is incomplete as the use of a constant void fraction implies that the pressure correction term in (16) is zero.

The results reported in Figures 2 and 3 show that, for Case 2, the fluid does not converge towards a static solution even though there is no driving force. It can also be drawn from Figures 3 and 4 that the magnitude of this spurious velocity is more important in regions of higher void fraction gradients.

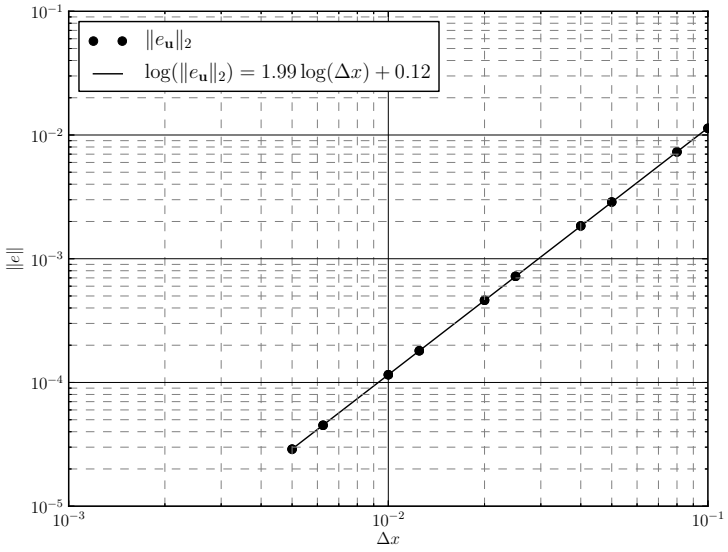

Figure 1: Euclidean norm of the error on $\boldsymbol{u}$ as a function of lattice spacing, and order of convergence for Case 1.

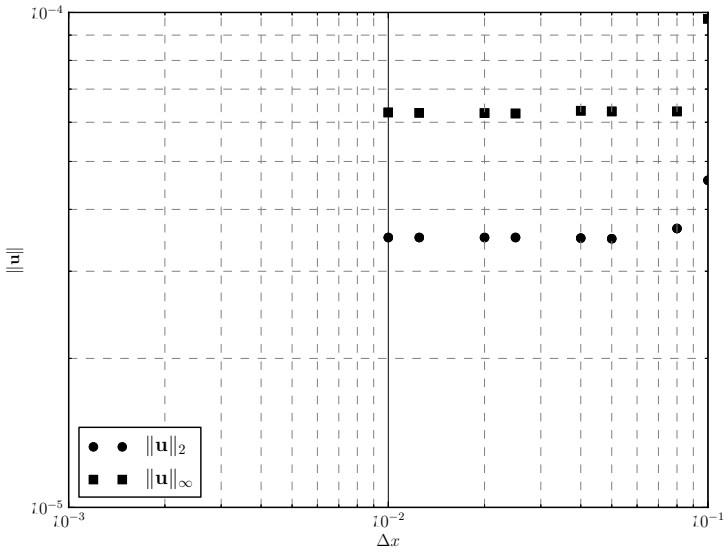

Figure 2: Euclidean and infinity norms of the velocity as a function of lattice spacing (Δx) for Case 2.

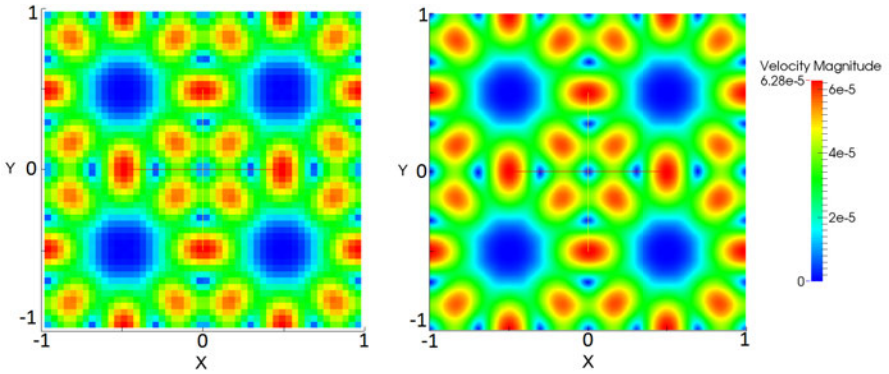

Figure 3: Magnitude of the velocity. Left panel: coarse grid (50×50) — Right panel: fine grid (200×200)

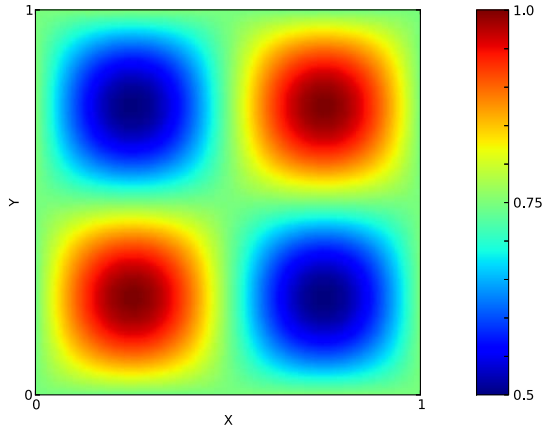

Figure 4: Void fraction ϵ_f for Case 2.

Case 3 highlights this last fact. In this test case, the analytical void fraction is a two-dimensional step function, which means that its gradient cannot converge towards a constant value, but rather increases as the grid is refined. Consequently, the velocity is expected to diverge as the grid is refined, which is what is observed in Figure 5. More precisely, it shows that the infinity norm of the error in velocity exhibits a first-order divergence with respect to grid spacing, which can be related to the increase of the void fraction gradient.

Finally, results for Cases 4 and 5 (not presented here) have further ascertained that the pressure-correction LBM-VANS scheme always yields a wrong velocity field when the void fraction is not constant. In fact, this scheme was

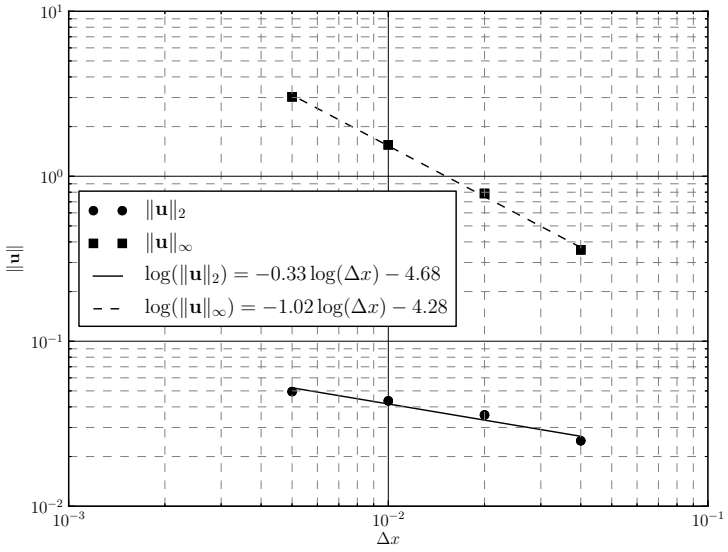

Figure 5: Euclidean and infinity norms of the velocity as a function of lattice spacing (Δx) for Case 3.

highly unstable for these two cases and most of the simulations could not converge due to numerical instabilities. This lack of robustness was amplified as the grid was refined, which prevented us from carrying any convergence study with these two cases.

All these results indicate that the pressure-correction LBM-VANS scheme is not adequate. The error arises from the pressure correction and the related additional forcing term in Eq. (16). More precisely, the pressure resulting solely from the collision operator is false in the presence of a void fraction gradient and the addition of a forcing term was shown in this section to lead to an inconsistent and unstable scheme. This also indicates that an adequate LBM scheme for the VANS equations, which should yield the correct pressure gradient through a proper collision operator, is needed. Such a scheme will be developed and verified in the following sections.

8. LBM formulation for the VANS equations using a novel collision operator

As previously shown, the instability of the pressure-correction LBM-VANS scheme stems from an incorrect discretization of the pressure. This can be corrected by introducing a new collision operator in which the population at rest

and the other populations are defined differently, thereby modifying the equation of state for the pressure. Such strategy has been used in multiphase LBM schemes such as the Shan-Chen model [34] or Rothman-Keller type schemes [26, 35].

We carry out our demonstration using Einstein's notation in 2D for the D2Q9 lattice, although it can straightforwardly be extended to 3D and other lattices. The main idea behind the scheme is to change the collision operator to obtain a pressure gradient term that does not include the void fraction (ϵ_f). The zeroth-, first- and second-order moments that we need to recover are:

$$\sum_i f_i^{eq} =: \rho_f^{(0)} = \rho_f \epsilon_f \tag{29}$$

$$\sum_i f_i^{eq} \xi_{i,\alpha} =: j_\alpha^{(0)} = \rho_f \epsilon_f u_\alpha \tag{30}$$

$$\sum_i f_i^{eq} \xi_{i,\alpha} \xi_{i,\beta} =: \Pi_{\alpha\beta}^{(0)} = (\rho_f - \rho_\infty)\, c_s^2 \delta_{\alpha\beta} + \rho_f \epsilon_f u_\alpha u_\beta \tag{31}$$

where ρ_∞ is an arbitrary constant, independent of time and space, which we will use to ensure the positivity of the population at rest f_0^{eq}. We define the equilibrium population f_i^{eq} as a second-order polynomial [36]:

$$f_0^{eq} = A_0 + D\boldsymbol{u} \cdot \boldsymbol{u} \tag{32}$$

$$f_i^{eq} = A_1 + B\boldsymbol{\xi}_i \cdot \boldsymbol{u} + C\left(\boldsymbol{\xi} \cdot \boldsymbol{u}\right)^2 + D\boldsymbol{u} \cdot \boldsymbol{u}, \;\; \forall \;\; i \in \; [1, 8] \tag{33}$$

Using these expression, Eqs. (29), (30) and (31) can be solved analytically, leading to the following expressions for the equilibrium populations:

$$f_0^{eq} = w_0 \left(\frac{9\rho_f \epsilon_f - 5\rho_f + 5\rho_\infty}{4} - \rho_f \epsilon_f \left(\frac{\boldsymbol{u} \cdot \boldsymbol{u}}{2c_s^2} \right) \right) \tag{34}$$

$$f_i^{eq} = w_i \left(\rho_f - \rho_\infty + \rho_f \epsilon_f \left(\frac{(\boldsymbol{\xi}_i \cdot \boldsymbol{u})}{c_s^2} + \frac{(\boldsymbol{\xi}_i \cdot \boldsymbol{u})^2}{2c_s^4} - \frac{\boldsymbol{u} \cdot \boldsymbol{u}}{2c_s^2} \right) \right), \ \forall \ i \in [1, 8] \tag{35}$$

If $\rho_\infty = 0$, the positivity of f_0^{eq} is not guaranteed for $\epsilon_f < \frac{5}{9}$. By choosing the constant ρ_∞ correctly, one can however ensure the positivity of this population for a wider range of void fractions. Since ρ_∞ is constant in both time and space, this corresponds to defining the pressure up to a different constant, but does not modify the pressure gradient, thus ensuring that the correct VANS equations are obtained.

The third-order moment of this scheme resulting from Eqs. (34) and (35), which will be used in the Chapman-Enskog analysis for the reconstruction of the viscous tensor arising from the non-equilibrium part of the populations, is:

$$\sum_i f_i \xi_{i,\alpha} \xi_{i,\beta} \xi_{i,\gamma} =: S^{(0)}_{\alpha\beta\gamma} = \rho_f \epsilon_f c_s^2 \left(u_\alpha \delta_{\beta\gamma} + u_\beta \delta_{\alpha\gamma} + u_\gamma \delta_{\alpha\beta} \right) \tag{36}$$

8.1. Chapman-Enskog analysis of the new LBM-VANS scheme

In this section, we carry out a Chapman-Enskog analysis for the new collision operator. As the first part of the Taylor expansion of the LBM equation and

the corresponding analysis are identical to those for the regular LBM scheme, they will be briefly presented. For a more detailed development, the reader is referred to [29, 36, 37]. However, as the derivation of the deviatoric stress tensor resulting from the second-order moment of the non-equilibrium populations is more subtle than in the classical analysis, it will be thoroughly derived.

We first recall the lattice Boltzmann equation (Eq. (4)), without the forcing term $\boldsymbol{G}_i$:

$$f_i\left(\boldsymbol{x}+\boldsymbol{\xi}_i\Delta t, t+\Delta t\right) - f_i\left(\boldsymbol{x},t\right) = \frac{1}{\bar{\tau}}\left(f_i^{eq}\left(\boldsymbol{x},t\right) - f_i\left(\boldsymbol{x},t\right)\right) \tag{37}$$

We begin by giving a Taylor expansion in time (Δt) and space (Δx) of the left-hand side of this equation, up to the second order:

$$\begin{aligned} f_i\left(\boldsymbol{x}+\boldsymbol{\xi}_i\Delta t, t+\Delta t\right) = {} & f_i\left(\boldsymbol{x},t\right) + \Delta t\partial_t\left(f_i\left(\boldsymbol{x},t\right)\right) \\ & + \Delta t\xi_{i,\alpha}\partial_\alpha\left(f_i\left(\boldsymbol{x},t\right)\right) + \frac{\Delta t^2}{2}\partial_t\partial_t\left(f_i\left(\boldsymbol{x},t\right)\right) \\ & + \Delta t^2\xi_{i,\alpha}\partial_\alpha\partial_t\left(f_i\left(\boldsymbol{x},t\right)\right) + \frac{\Delta t^2}{2}\xi_{i,\alpha}\xi_{i,\beta}\partial_\alpha\partial_\beta\left(f_i\left(\boldsymbol{x},t\right)\right) \end{aligned} \tag{38}$$

We then carry out a classical Chapman-Enskog multiple time-scale analysis using an expansion parameter λ that is related to the Knudsen number.

Introducing the following populations and differential operators:

$$f_i =: f_i^{(0)} + \lambda f_i^{(1)} + \lambda^2 f_i^{(2)} =: f_i^{(0)} + \lambda f_i^{neq} \tag{39}$$

$$f_i^{neq} =: f_i^{(1)} + \lambda f_i^{(2)} \tag{40}$$

$$\partial_t =: \lambda \frac{\partial}{\partial t_1} + \lambda^2 \frac{\partial}{\partial t_2} =: \lambda \partial_t^{(1)} + \lambda^2 \partial_t^{(2)} \tag{41}$$

$$\partial_\alpha =: \lambda \partial_\alpha^{(1)} \tag{42}$$

and regrouping the terms in Eq. (38) by the order of λ, we find by substitution into Eq. (37):

$$\mathcal{O}\left(\lambda^0\right) : 0 = -\omega \left(f_i^{(0)} - f_i^{eq}\right) \tag{43}$$

$$\mathcal{O}\left(\lambda^1\right) : \partial_t^{(1)} f_i^{(0)} + \xi_{i,\alpha} \partial_\alpha^{(1)} f_i^{(0)} = -\frac{\omega}{\Delta t} f_i^{(1)} \tag{44}$$

$$\mathcal{O}\left(\lambda^2\right) : \partial_t^{(2)} f_i^{(0)} + \left(1 - \frac{\omega}{2}\right) \left(\partial_t^{(1)} f_i^{(1)} + \xi_{i,\alpha} \partial_\alpha^{(1)} f_i^{(1)}\right) = -\frac{\omega}{\Delta t} f_i^{(2)} \tag{45}$$

where $\omega = \frac{1}{\tau}$. Using Eq. (43), we can identify $f_i^{(0)}$ with f_i^{eq}. Next, we impose the following constraints on the non-equilibrium populations [29, 36, 38]:

$$\sum_i f_i^{(k)} = 0, \ \ \forall \ \ k > 0 \tag{46}$$

$$\sum_i f_i^{(k)} \xi_i = 0, \ \ \forall \ \ k > 0 \tag{47}$$

We can next calculate the zeroth-, first- and second-order moments of Eq. (44) in order to recover the equations for the conserved moments. To do so, we

define:

$$\sum_i f_i^{(k)} =: \rho_f^{(k)} \tag{48}$$

$$\sum_i f_i^{(k)} \xi_{i,\alpha} =: j_\alpha^{(k)} \tag{49}$$

$$\sum_i f_i^{(k)} \xi_{i,\alpha} \xi_{i,\beta} =: \Pi_{\alpha\beta}^{(k)} \tag{50}$$

$$\sum_i f_i^{(k)} \xi_{i,\alpha} \xi_{i,\beta} \xi_{i,\gamma} =: S_{\alpha\beta\gamma}^{(k)} \tag{51}$$

It follows from, Eqs. (46) and (48), and Eqs.(47) and (49), respectively, that :

$$\rho_f^{(k)} = 0 \ \ \forall \ \ k > 0 \tag{52}$$

$$j_\alpha^{(k)} = 0 \ \ \forall \ \ k > 0 \tag{53}$$

From the moments of Eq. (44), we then get:

$$\sum_i \rightarrow \ \partial_t^{(1)} \left(\rho_f \epsilon_f\right) + \partial_\alpha^{(1)} \left(\rho_f \epsilon_f u_\alpha\right) = 0 \tag{54}$$

$$\sum_i \xi_{i,\alpha} \rightarrow \ \partial_t^{(1)} \left(\rho_f \epsilon_f u_\alpha\right) + \partial_\beta^{(1)} \left(\rho_f \epsilon_f u_\alpha u_\beta\right) + \partial_\alpha^{(1)} (\rho_f - \rho_\infty) c_s^2 = 0 \tag{55}$$

$$\sum_i \xi_{i,\alpha} \xi_{i,\beta} \rightarrow \ \partial_t^{(1)} \left(\Pi_{\alpha\beta}^{(0)}\right) + \partial_\gamma^{(1)} \left(S_{\alpha\beta\gamma}^{(0)}\right) = -\frac{\omega}{\Delta t} \Pi_{\alpha\beta}^{(1)} \tag{56}$$

Applying the same procedure to Eq. (45), we obtain:

$$\sum_i \rightarrow \ \partial_t^{(2)} \left(\rho_f \epsilon_f\right) = 0 \tag{57}$$

$$\sum_i \xi_{i,\alpha} \rightarrow \ \partial_t^{(2)} \left(\rho_f \epsilon_f u_\alpha\right) + \left(1 - \frac{\omega}{2}\right) \partial_\beta^{(1)} \left(\Pi_{\alpha\beta}^{(1)}\right) = 0 \tag{58}$$

Next, following along the lines of Guo and Shu [29] for the standard LBM scheme, the zeroth- (Eqs. (54) and (57)) and first-order (Eqs. (55) and (58)) moment equations on the λ and λ^2 scales can be combined to yield:

$$\partial_t \left(\rho_f \epsilon_f\right) + \partial_\alpha \left(\rho_f \epsilon_f u_\alpha\right) = 0 \tag{59}$$

$$\partial_t \left(\rho_f \epsilon_f u_\alpha\right) + \partial_\beta \left(\rho_f \epsilon_f u_\alpha u_\beta\right) + \partial_\beta \left(\left(\rho_f - \rho_\infty\right) c_s^2 \delta_{\alpha\beta}\right) = -\lambda \left(1 - \frac{\omega}{2}\right) \partial_\beta \left(\Pi_{\alpha\beta}^{(1)}\right) \tag{60}$$

where ∂_t and ∂_β are defined in Eqs. (41) and (42). It is then necessary to close the Chapman-Enskog expansion and calculate the second-order moment of the non-equilibrium populations, which will be linked to the deviatoric stress tensor. As is the case in the classical analysis [29], the second-order moment of the non-equilibrium populations, Eq. (56), is given by:

$$-\frac{\omega}{\Delta t} \Pi_{\alpha\beta}^{(1)} = \partial_t^{(1)} \left(\Pi_{\alpha\beta}^{(0)}\right) + \partial_\gamma^{(1)} \left(S_{\alpha\beta\gamma}^{(0)}\right) \tag{61}$$

We recall that the second-order and third-order moments of the equilibrium populations, Eqs. (31) and (36), are:

$$\Pi_{\alpha\beta}^{(0)} = \left(\rho_f - \rho_\infty\right) c_s^2 \delta_{\alpha\beta} + \rho_f \epsilon_f u_\alpha u_\beta \tag{62}$$

$$S_{\alpha\beta\gamma}^{(0)} = \rho_f \epsilon_f c_s^2 \left(u_\alpha \delta_{\beta\gamma} + u_\beta \delta_{\alpha\gamma} + u_\gamma \delta_{\alpha\beta}\right) \tag{63}$$

Combining Eqs. (61), (62) and (63) leads to:

$$-\frac{\omega}{\Delta t}\Pi_{\alpha\beta}^{(1)} = \partial_t^{(1)}\left(\left(\rho_f - \rho_\infty\right)c_s^2\delta_{\alpha\beta}\right) + \partial_t^{(1)}\left(\rho_f\epsilon_f u_\alpha u_\beta\right) + \partial_\gamma^{(1)}\left(\rho_f\epsilon_f c_s^2\left(u_\alpha\delta_{\beta\gamma} + u_\beta\delta_{\alpha\gamma} + u_\gamma\delta_{\alpha\beta}\right)\right) \tag{64}$$

One problem in this expression is that ρ_f is not a conserved moment and that no state equation for $\partial_t^{(1)}\rho_f$ exists. In order to use the classical LBM scheme demonstration, we can rewrite Eq. (64) in the following form, by first adding and subtracting $\partial_t^{(1)}\left(\rho_f\epsilon_f c_s^2\delta_{\alpha\beta}\right)$ to its right-hand side, and then eliminating the term involving constant ρ_∞ as its derivative is zero:

$$-\frac{\omega}{\Delta t}\Pi_{\alpha\beta}^{(1)} = \underbrace{\partial_t^{(1)}\left(\rho_f\epsilon_f c_s^2\delta_{\alpha\beta}\right)}_{I} + \underbrace{\partial_t^{(1)}\left(\rho_f\epsilon_f u_\alpha u_\beta\right)}_{II} + \underbrace{\partial_\gamma^{(1)}\left(\rho_f\epsilon_f c_s^2\left(u_\alpha\delta_{\beta\gamma} + u_\beta\delta_{\alpha\gamma} + u_\gamma\delta_{\alpha\beta}\right)\right)}_{III} + \underbrace{\partial_t^{(1)}\left(\rho_f c_s^2\delta_{\alpha\beta}\right) - \partial_t^{(1)}\left(\rho_f\epsilon_f c_s^2\delta_{\alpha\beta}\right)}_{IV} \tag{65}$$

Using the conservation equations for the zeroth- and first-order moments of the equilibrium populations, Eqs. (54) and (55), the time derivatives of the conserved moments ($\rho_f^{(0)} = \rho_f\epsilon_f$) and ($j_\alpha^{(0)} = \rho_f\epsilon_f u_\alpha$) can be expressed as:

$$\partial_t^{(1)}\left(\rho_f\epsilon_f\right) = -\partial_\gamma^{(1)}\left(\rho_f\epsilon_f u_\gamma\right) \tag{66}$$

$$\partial_t^{(1)}\left(\rho_f\epsilon_f u_\alpha\right) = -\partial_\alpha^{(1)}\left(\rho_f c_s^2\right) - \partial_\gamma^{(1)}\left(\rho_f\epsilon_f u_\alpha u_\gamma\right) \tag{67}$$

which enables us to rewrite the right-hand side of Eq. (65). We initially focus on terms (I, II, III) of this equation as their treatment is similar to the case of the classical LBM scheme. By distributing the derivatives, we get:

$$\begin{aligned}-\frac{\omega}{\Delta t}\Pi_{\alpha\beta}^{(1)} =&\partial_t^{(1)}\left(\rho_f\epsilon_f\right)\delta_{\alpha\beta}c_s^2 \\ &+\frac{j_\beta}{\rho_f\epsilon_f}\partial_t^{(1)}\left(j_\alpha\right)+\frac{j_\alpha}{\rho_f\epsilon_f}\partial_t^{(1)}\left(j_\beta\right)-\frac{j_\alpha j_\beta}{\left(\rho_f\epsilon_f\right)^2}\partial_t^{(1)}\left(\rho_f\epsilon_f\right) \\ &+\partial_\gamma^{(1)}\left(\rho_f\epsilon_f c_s^2\left(u_\alpha\delta_{\beta\gamma}+u_\beta\delta_{\alpha\gamma}+u_\gamma\delta_{\alpha\beta}\right)\right)+IV\end{aligned} \tag{68}$$

Simplifying the mass and momentum terms using Eqs. (66) and (67), it follows that:

$$\begin{aligned}-\frac{\omega}{\Delta t}\Pi_{\alpha\beta}^{(1)} =&-\partial_\gamma^{(1)}\left(\rho_f\epsilon_f u_\gamma\right)\delta_{\alpha\beta}c_s^2 \\ &-u_\beta\left(\partial_\alpha^{(1)}\left(\rho_f c_s^2\right)+\partial_\gamma^{(1)}\left(\rho_f\epsilon_f u_\alpha u_\gamma\right)\right) \\ &-u_\alpha\left(\partial_\beta^{(1)}\left(\rho_f c_s^2\right)+\partial_\gamma^{(1)}\left(\rho_f\epsilon_f u_\beta u_\gamma\right)\right) \\ &+u_\alpha u_\beta\partial_\gamma^{(1)}\left(\rho_f\epsilon_f u_\gamma\right) \\ &+\partial_\gamma^{(1)}\left(\rho_f\epsilon_f c_s^2\left(u_\alpha\delta_{\beta\gamma}+u_\beta\delta_{\alpha\gamma}+u_\gamma\delta_{\alpha\beta}\right)\right)+IV\end{aligned} \tag{69}$$

Tedious but simple calculus then leads to:

$$\begin{aligned}-\frac{\omega}{\Delta t}\Pi_{\alpha\beta}^{(1)} =&\rho_f\epsilon_f\partial_\alpha^{(1)}\left(u_\beta\right)c_s^2+\rho_f\epsilon_f\partial_\beta^{(1)}\left(u_\alpha\right)c_s^2-\partial_\gamma^{(1)}\left(\rho_f\epsilon_f u_\alpha u_\beta u_\gamma\right) \\ &+u_\alpha\left(\partial_\beta^{(1)}\left(\rho_f\epsilon_f c_s^2\right)-\partial_\beta^{(1)}\left(\rho_f c_s^2\right)\right)+u_\beta\left(\partial_\alpha^{(1)}\left(\rho_f\epsilon_f c_s^2\right)-\partial_\alpha^{(1)}\left(\rho_f c_s^2\right)\right) \\ &+IV\end{aligned} \tag{70}$$

Next, we can rearrange term IV in Eq. (70) using Eq. (54), to obtain the final form of the viscous stress tensor. The resulting equation, which is consistent with the classical LBM scheme, is:

$$
\begin{aligned}
-\frac{\omega}{\Delta t}\Pi^{(1)}_{\alpha\beta} =& \rho_f\epsilon_f\partial^{(1)}_{\alpha}\left(u_\beta\right)c_s^2 + \rho_f\epsilon_f\partial^{(1)}_{\beta}\left(u_\alpha\right)c_s^2 - \partial^{(1)}_{\gamma}\left(\rho_f\epsilon_f u_\alpha u_\beta u_\gamma\right) \\
&+ u_\alpha\left(\partial^{(1)}_{\beta}\left(\rho_f\epsilon_f c_s^2\right) - \partial^{(1)}_{\beta}\left(\rho_f c_s^2\right)\right) + u_\beta\left(\partial^{(1)}_{\alpha}\left(\rho_f\epsilon_f c_s^2\right) - \partial^{(1)}_{\alpha}\left(\rho_f c_s^2\right)\right) \\
&+ \partial^{(1)}_{\gamma}\left(\rho_f\epsilon_f u_\gamma\right)c_s^2\delta_{\alpha\beta} - c_s^2\left(\frac{\partial^{(1)}_{\gamma}\left(\rho_f\epsilon_f u_\gamma\right) + \rho_f\partial^{(1)}_{t}\left(\epsilon_f\right)}{\epsilon_f}\right) \qquad (71)
\end{aligned}
$$

This simplification of term IV leads to an expression with no time derivatives for ρ_f, thereby eliminating the need to store this variable at two consecutive iterations in order to maintain the second-order accuracy of the scheme.

Combining Eqs. (8), (60) and (71), and simplifying the resulting expression leads to:

$$
\partial_t\left(\rho_f\epsilon_f u_\alpha\right) + \partial_\beta\left(\rho_f\epsilon_f u_\alpha u_\beta\right) + \partial_\beta\left(\left(\rho_f - \rho_\infty\right)c_s^2\delta_{\alpha\beta}\right) = \partial_\beta\left(\Theta_{\alpha\beta}\right) \qquad (72)
$$

where $\Theta_{\alpha\beta}$ is defined as:

$$\begin{aligned}\Theta_{\alpha\beta} =& \underbrace{\mu\epsilon_f\partial_\alpha\left(u_\beta\right) + \mu\epsilon_f\partial_\beta\left(u_\alpha\right)}_{i} - \underbrace{\frac{\mu}{\rho_f c_s^2}\partial_\gamma\left(\rho_f\epsilon_f u_\alpha u_\beta u_\gamma\right)}_{ii} \\ &+ \underbrace{\frac{\mu}{\rho_f}\left(u_\alpha\left(\partial_\beta\left(\rho_f\epsilon_f\right) - \partial_\beta\left(\rho_f\right)\right) + u_\beta\left(\partial_\alpha\left(\rho_f\epsilon_f\right) - \partial_\alpha\left(\rho_f\right)\right)\right)}_{iii} \\ &+ \underbrace{\frac{\mu}{\rho_f}\partial_\gamma\left(\rho_f\epsilon_f u_\gamma\right)\delta_{\alpha\beta} - \frac{\mu}{\rho_f}\left(\frac{\partial_\gamma\left(\rho_f\epsilon_f u_\gamma\right) + \rho_f\partial_t\left(\epsilon_f\right)}{\epsilon_f}\right)}_{iv}\end{aligned} \tag{73}$$

We recall that the deviatoric stress tensor of the VANS equations is [7]:

$$D_{\alpha\beta} = \epsilon_f\mu\left(\partial_\alpha\left(u_\beta\right) + \partial_\beta\left(u_\alpha\right) - \underbrace{\frac{2}{3}\partial_\gamma\left(u_\gamma\right)\delta_{\alpha\beta}}_{v}\right) \tag{74}$$

It can be seen by comparing Eqs. (73) and (74) that the viscous stress tensor that arises from the new collision operator and its underlying equilibrium populations, Eqs. (34) and (35), is not consistent with the one from the VANS equations. More precisely, term (i) is the classical deviatoric stress tensor that is present in the regular LBM scheme (with $\epsilon_f = 1$). Term (ii) is also present in the regular LBM scheme and is considered to be asymptotically vanishing with the Mach number. Terms (iii) and (iv) do not exist in the regular LBM scheme. Finally, term (v) of the deviatoric stress tensor is missing in Eq. (73). Note that this term is also absent in the regular LBM scheme. In the latter, the velocity field is asymptotically divergence free in the incompressible limit so

that this term vanishes. This is not the case for the VANS equations.

We can conclude from the above discussion that the viscous stress tensor arising from the new LBM-VANS scheme is not valid without modifications; terms (iii) and (iv) must be removed and term (v) must be added. This can be accomplished by the addition of an appropriate forcing term to the formulation.

Following Eqs. (59) and (72), the resulting equations for the new scheme are:

$$\partial_t \left(\rho_f \epsilon_f\right) + \partial_\gamma \left(\rho_f \epsilon_f u_\gamma\right) = 0 \tag{75}$$

$$\partial_t \left(\rho_f \epsilon_f u_\alpha\right) + \partial_\gamma \left(\rho_f \epsilon_f u_\gamma u_\alpha\right) = -\nabla \left(\rho_f c_s^2\right) + \partial_\beta \left(\Theta_{\alpha\beta}\right) - \partial_\beta \left(\Theta_{\alpha\beta}^C\right) + F_\alpha^P \tag{76}$$

where $\Theta_{\alpha\beta}^C$ is a correction tensor defined as:

$$\begin{aligned}\Theta_{\alpha\beta}^C =& \frac{\mu u_\alpha}{\rho_f}\left(\partial_\beta \left(\rho_f \epsilon_f\right) - \partial_\beta \left(\rho_f\right)\right) + \frac{\mu u_\beta}{\rho_f}\left(\partial_\alpha \left(\rho_f \epsilon_f\right) - \partial_\alpha \left(\rho_f\right)\right) \\ &+ \frac{\mu}{\rho_f}\partial_\gamma \left(\rho_f \epsilon_f u_\gamma\right)\delta_{\alpha\beta} - \frac{\mu}{\rho_f \epsilon_f}\left(\partial_\gamma \left(\rho_f \epsilon_f u_\gamma\right) + \rho_f \partial_t \left(\epsilon_f\right)\right) \\ &+ \frac{2}{3}\mu \epsilon_f \partial_\gamma \left(u_\gamma\right)\delta_{\alpha\beta}\end{aligned} \tag{77}$$

F_α^P is a pressure correction force term needed to recoved $\epsilon_f \nabla p$:

$$F_\alpha^P = (1 - \epsilon_f)\partial_\alpha \left(\rho_f c_s^2\right) \tag{78}$$

Eqs. (75) and (76) are asymptotically equivalent to the following VANS equa-

tions:

$$\frac{\partial \epsilon_f}{\partial t} + \nabla \cdot (\epsilon_f \boldsymbol{u}) = 0 \tag{79}$$

$$\frac{\partial (\rho_f \epsilon_f \boldsymbol{u})}{\partial t} + \nabla \cdot (\rho_f \epsilon_f \boldsymbol{u} \otimes \boldsymbol{u}) = -\epsilon_f \nabla p + \nabla \cdot \boldsymbol{\tau} \tag{80}$$

We note that the correction tensor, $\Theta^C_{\alpha\beta}$, is well-posed as it is only dependent on μ, ρ_f, ϵ_f, $\boldsymbol{u}$ and their derivatives. Therefore, it converges towards a constant value when the grid is refined. This is why this scheme is different from the pressure-correction LBM-VANS scheme of Section 4, and why it should solve adequately the no-flow tests of Sections 6.2 and 6.3. Furthermore, the regular lattice Boltzmann method is recovered when $\epsilon_f = 1$. Consequently, the scheme is consistent with the classical implementation of the LBM.

In practice, the additional source terms in Eq. (76) are calculated outside the collision step (Eq. (11)). They involve first- and second-order derivatives, which are approximated by means of a standard second-order finite difference formula. Moreover, the divergence of the correction tensor (Eq. (77)), which is required in Eq. (76), involves the calculation of $\partial_\alpha \partial_\beta \epsilon_f$ with $\alpha \neq \beta$. This is done on the LBM structured grid (with $\Delta x = \Delta y$) using the following diagonal

stencil:

$$\frac{\partial^2 \epsilon_f(x,y,t)}{\partial\alpha\partial\beta} = \frac{\epsilon_f(\alpha+\Delta x,\beta+\Delta x,t)+\epsilon_f(\alpha-\Delta x,\beta-\Delta x,t)}{4\Delta x^2} - \left(\frac{\epsilon_f(\alpha-\Delta x,\beta+\Delta x,t)+\epsilon_f(\alpha+\Delta x,\beta-\Delta x,t)}{4\Delta x^2}\right) \quad (81)$$

9. Results with the LBM-VANS scheme and the new collision operator

We present the results obtained with the LBM-VANS scheme introduced in the previous section for the five different test cases. Figures 6, 7 and 8 display the evolution of the Euclidean norm of the error on $\boldsymbol{u}$ as a function of the lattice spacing for Cases 1, 4 and 5. These three graphs show that the velocity exhibits second-order convergence even for the most complex manufactured solution (Case 5), which involves a complete non-zero viscous stress tensor. It should be recalled that the pressure-correction LBM-VANS scheme of Section 4 was not stable for Cases 4 and 5, causing a blow-up of the simulations. As predicted by the theoretical analysis done in Section 8.1, the new LBM-VANS scheme and its underlying corrective source terms converges towards the desired form of the VANS equations up to the second-order. Furthermore, the scheme exhibits very good mass conservation properties as the average density was preserved up to 10^{-14} kg.m^{-3} upon convergence in all simulations. We note that

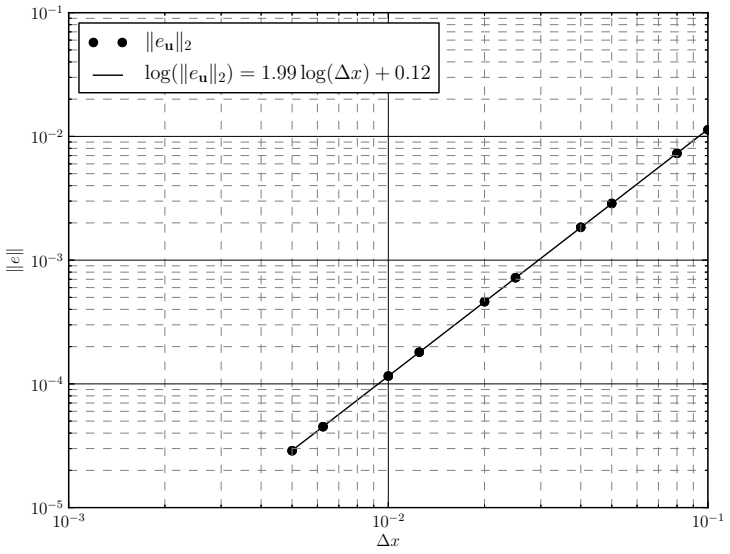

Figure 6: Euclidean norm of the error on the velocity as a function of lattice spacing, and order of convergence for Case 1 with the new LBM-VANS scheme.

the results obtained for Cases 1 in Figure 6 are identical to those obtained with the pressure-correction scheme in Figure 1. For a constant void fraction, as is the case in Case 1, all the source terms are zero and, consequently, both schemes give identical results.

Next, Figures 9 and 10 show that the velocity for the two no-flow tests (Cases 2 and 3) is negligible for all grids ($|\boldsymbol{u}| < 10^{-11}$ m.s^{-1}). We consider that this is an essential property that any scheme should possess as it indicates that it does not create kinetic energy in the absence of fluid flow. However, we

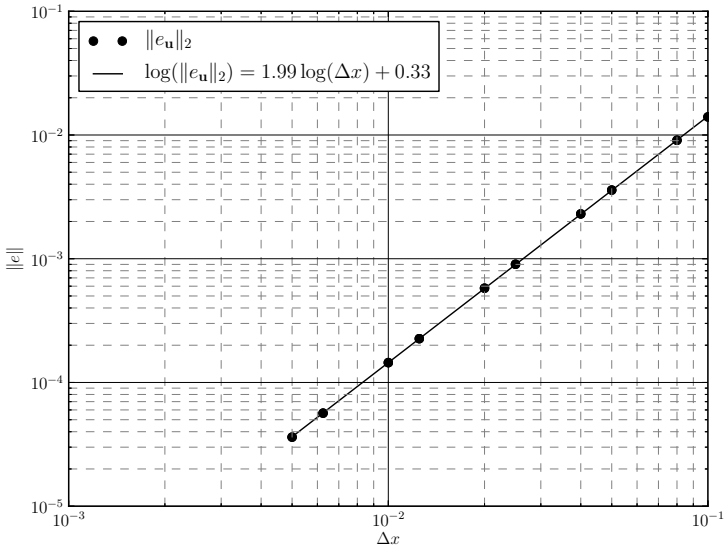

Figure 7: Euclidean norm of the error on the velocity as a function of lattice spacing, and order of convergence for Case 4 with the new LBM-VANS scheme.

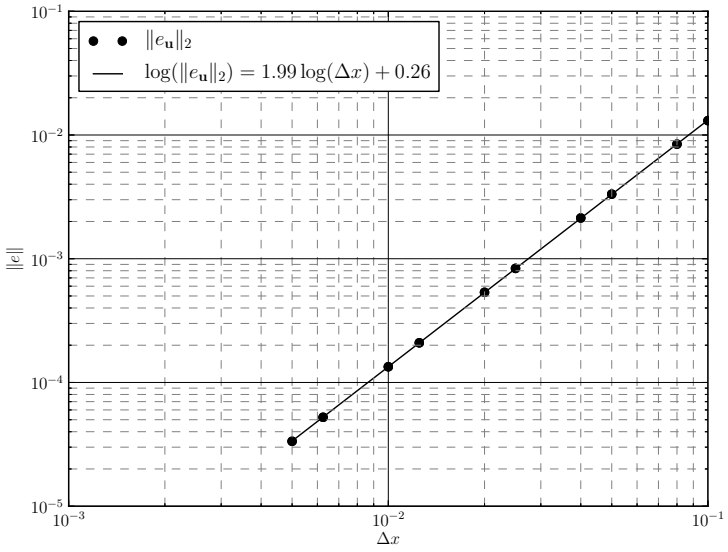

Figure 8: Euclidean norm of the error on the velocity as a function of lattice spacing, and order of convergence for Case 5 with the new LBM-VANS scheme.

note that, although the spurious velocities in these two figures are negligible, their magnitude increases when the grid is refined. This is due to the fact that our code uses SI units instead of lattice units. Therefore the lattice speed of sound, c_s, increases when Δx decreases under diffusive scaling. Indeed, the only remaining source term in this case comes from Eq. (78), and its magnitude is related to the numerical error (floating point operations) in the centered finite difference formula for the evaluation of $\partial_\alpha \rho_f$. This term, which is multiplied by the lattice speed of sound squared (c_s^2), is responsible for these spurious but very small velocities.

Some comments are in order concerning the stability of the new scheme. We have found that, for low void fractions ($\epsilon_f < 0.45$), the model suffers from a pressure checkerboard effect, leading to instabilities and loss of convergence. This lower bound for stability increases to $\epsilon_f = 0.55$ for small relaxation times ($\bar{\tau} \in]0.5, 0.51]$). Note that this behavior is unaffected by the variation of parameter ρ_∞. Although results were observed for 10^4 lattice grids ($\Delta x = 0.02$), this behavior was not affected significantly by the lattice spacing and could not be eliminated by refining or coarsening the grid.

A straightforward solution to this problem consists of rescaling the density and void fraction so that they lie in the stability range of the scheme, while

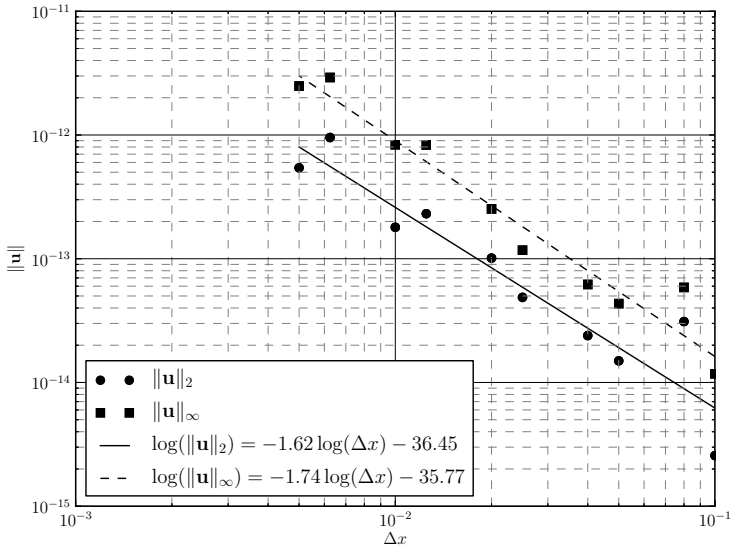

Figure 9: Euclidean and infinity norms of the velocity as a function of lattice spacing (Δx) for Case 2 with the new LBM-VANS scheme.

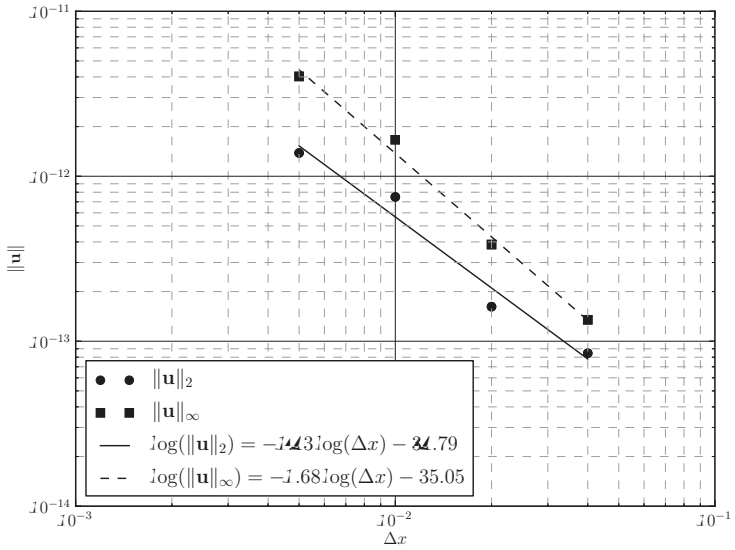

Figure 10: Euclidean and infinity norms of the velocity as a function of lattice spacing (Δx) for Case 3 with the new LBM-VANS scheme.

maintaining a constant mass per lattice cell. To do so, we introduce a density $\rho_{f,1}$ and void fraction $\epsilon_{f,1}$ such that :

$$\rho_{f,1}\epsilon_{f,1} = \rho\epsilon_f = \bar{\rho} \tag{82}$$

with $\epsilon_{f,1} > \epsilon_f$ and $\rho_{f,1} < \rho_f$. For instance, one could take $\rho_{f,1} = \frac{\rho_f}{\theta}$ and $\epsilon_{f,1} = \theta\epsilon_f$, so that $\epsilon_{f,1} > 0.45$, thus ensuring the stability of the scheme. We have found that, even for large values of ϵ_f such as $\epsilon_f = 3$ and for large variations of ϵ_f such as $max(\epsilon_f) - min(\epsilon_f) = 2.5$, the scheme remains stable, mass conservative and second-order accurate for all grid sizes.

10. Conclusion

The volume-averaged Navier-Stokes equations are commonly used for the modeling of multiphase flows in industrial applications. Indeed, they are part of numerous approaches in which they describe either all phases, as in two-fluid models, or the suspending fluid only, as in the case of unresolved CFD-DEM models.

The VANS equations are traditionally solved by means of the finite volume method or the finite element method. However, the lattice Boltzmann method is an interesting alternative to solve these equations because it is fully explicit,

easily parallelizable owing to its local operations, and second-order accurate.

In the literature, the use of the LBM to solve the VANS equations has been done by means of two approaches. The first one is based on a modified collision operator and a pressure correction forcing term [18, 19, 20]. As we have shown in the present work, this method does not solve adequately the no-flow test (Cases 2 and 3), and is unstable in the case of problems involving void fraction gradients (Cases 4 and 5). The other type of implementation of the VANS equations within the LBM has been done using additional mass and momentum source terms [17]. However, this approach had not been shown to be second-order accurate, is more computationally intensive, requires sub-iterations and does not solve the VANS equation in a conservative formulation.

In this work, a VANS model for the lattice Boltzmann method based on a new collision operator involving two correction terms has been proposed. It is fully explicit and requires the same stencil as the classical lattice Boltzmann scheme. A Chapman-Enskog analysis has proven that the VANS equations are recovered with the correct deviatoric stress tensor. By designing analytical test cases using the method of manufactured solutions, this model has been shown to be second-order accurate for complex 2D cases, something that, to our knowledge, had never been done with other LBM-VANS models. Furthermore,

the results obtained with the no-flow tests have revealed that this model predicts the pressure adequately.

Although our model suffers *a priori* from a stability problems at low void fractions, a slight modification entailing a rescaling of the density and void fraction has been observed to be an efficient workaround. Furthermore, this model is stable for very large void fraction gradients, which represents a significant improvement over current models.

Future work includes the extension of the model to 3D using D3Q19 lattices, which is a natural extension of the D2Q9 scheme within the scope of flows in porous media or solid-fluid flows using a CFD-DEM combination.

11. Acknowledgements

The financial support from the Natural Sciences and Engineering Research Council of Canada (NSERC) is gratefully acknowledged. In particular, Bruno Blais is thankful for the NSERC Vanier Scholarship. The authors would also like to acknowledge the technical support and computing time provided by Compute Canada. Finally, the authors would like to thank Pr. Dominique Pelletier from Polytechnique Montréal for fruitful and enlightening discussions on the method of manufactured solutions.

References

[1] E. L. Paul, V. A. Atiemo-Obeng, S. M. Kresta, Handbook of Industrial Mixing - Science and Practice (2004).

[2] C. Crowe, J. D. Schwartzkopf, M. Sommerfeld, Y. Tsuji, Multiphase Flows with Droplets and Particles Flows, CRC Press, 2012.

[3] H. P. Zhu, Z. Y. Zhou, R. Y. Yang, A. B. Yu, Discrete particle simulation of particulate systems: A review of major applications and findings, Chemical Engineering Science 63 (23) (2008) 5728–5770.

[4] Y. Tsuji, Multi-scale modeling of dense phase gas-particle flow, Chemical Engineering Science 62 (13) (2007) 3410–3418.

[5] T. B. Anderson, R. Jackson, Fluid mechanical description of fluidized beds. Equations of motion, Industrial & Engineering Chemistry Fundamentals 6 (4) (1967) 527–539.

[6] D. Gidaspow, Multiphase Flow and Fluidization: Continuum and Kinetic Theory Descriptions, Academic press, 1994.

[7] H. P. Zhu, Z. Y. Zhou, R. Y. Yang, A. B. Yu, Discrete particle simulation

of particulate systems: Theoretical developments, Chemical Engineering Science 62 (13) (2007) 3378–3396.

[8] D. M. Snider, An incompressible three-dimensional multiphase particle-in-cell model for dense particle flows, Journal of Computational Physics 170 (2) (2001) 523–549.

[9] A. Tamburini, A. Brucato, A. Cipollina, G. Micale, M. Ciofalo, CFD predictions of sufficient suspension conditions in solid-liquid agitated tanks, International Journal of Nonlinear Sciences and Numerical Simulation 13 (6) (2012) 427–443.

[10] R. E. Hayes, A. Afacan, B. Boulanger, An equation of motion for an incompressible Newtonian fluid in a packed bed, Transport in Porous Media 18 (2) (1995) 185–198.

[11] Z. Y. Zhou, S. B. Kuang, K. W. Chu, A. B. Yu, Discrete particle simulation of particle-fluid flow: model formulations and their applicability, Journal of Fluid Mechanics 661 (2010) 482–510.

[12] A. Di Renzo, F. Cello, F. P. Di Maio, Simulation of the layer inversion phenomenon in binary liquid-fluidized beds by DEM-CFD with a drag law for

polydisperse systems, Chemical Engineering Science 66 (13) (2011) 2945–2958.

[13] K. D. Kafui, C. Thornton, M. J. Adams, Discrete particle-continuum fluid modelling of gas-solid fluidised beds, Chemical Engineering Science 57 (13) (2002) 2395–2410.

[14] R. Garg, J. Galvin, T. Li, S. Pannala, Open-source MFIX-DEM software for gas-solids flows: Part I verification studies, Powder Technology 220 (2012) 122–137.

[15] P. Pepiot, O. Desjardins, Numerical analysis of the dynamics of two- and three-dimensional fluidized bed reactors using an Euler-Lagrange approach, Powder Technology 220 (2012) 104–121.

[16] M. Robinson, M. Ramaioli, S. Luding, Fluid–particle flow simulations using two-way-coupled mesoscale SPH-DEM and validation, International Journal of Multiphase Flow 59 (2014) 121–134.

[17] F. Song, W. Wang, J. Li, A lattice Boltzmann method for particle-fluid two-phase flow, Chemical Engineering Science 102 (2013) 442–450.

[18] T. F. Wang, J. F. Wang, Two-fluid model based on the lattice Boltzmann equation, Physical Review E 71 (4).

[19] Q. Xiong, E. Madadi-Kandjani, G. Lorenzini, A LBM-DEM solver for fast discrete particle simulation of particle-fluid flows, Continuum Mechanics and Thermodynamics (2014) 1–11.

[20] J. Zhang, L. Wang, J. Ouyang, Lattice Boltzmann model for the volume-averaged Navier-Stokes equations, EPL (Europhysics Letters) 107 (2) (2014) 20001.

[21] B. Blais, F. Bertrand, On the use of the method of manufactured solutions for the verification of CFD codes for the volume-averaged Navier-Stokes equations, Submitted to Computers & Fluids.

[22] CFDEM, CFDEM: Open Source CFD, DEM and CFD-DEM, URL : http://www.cfdem.com, 2014, visited on 2014-12-08.

[23] OpenCFD, OpenFOAM - The Open Source CFD Toolbox, URL : http://www.openfoam.com, 2014, visited on 2014-12-08.

[24] LIGGGHTS, LAMMPS Improved for General Granular and Granular Heat

Transfer Simulations, URL : hhtp://www.liggghts.com, 2014, visited on 2014-12-08.

[25] C. Kloss, C. Goniva, LIGGGHTS–Open Source Discrete Element Simulations of Granular Materials Based on Lammps, Wiley Online Library, 2011, pp. 781–788.

[26] S. Leclaire, M. Reggio, J.-Y. Trépanier, Isotropic color gradient for simulating very high-density ratios with a two-phase flow lattice Boltzmann model, Computers & Fluids 48 (1) (2011) 98–112.

[27] M. Meldi, E. Vergnault, P. Sagaut, An arbitrary Lagrangian-Eulerian approach for the simulation of immersed moving solids with lattice Boltzmann method, Journal of Computational Physics 235 (2013) 182–198.

[28] S. Succi, The Lattice Boltzmann Equation: For Fluid Dynamics and Beyond, Oxford University Press on Demand, 2001.

[29] Z. Guo, C. Shu, Lattice Boltzmann Method and Its Applications in Engineering, World Scientific Publishing Company Incorporated, 2013.

[30] P. L. Bhatnagar, E. P. Gross, M. Krook, A model for collision processes in

gases. I. Small amplitude processes in charged and neutral one-component systems, Physical Review 94 (3) (1954) 511–525.

[31] P. Lallemand, L. S. Luo, Theory of the lattice Boltzmann method: Dispersion, dissipation, isotropy, Galilean invariance, and stability, Physical Review E 61 (6) (2000) 6546–6562.

[32] W. Oberkampf, C. Roy, Verification and Validation in Scientific Computing, Cambridge University Press, 2010.

[33] Wolfram Research, Mathematica, 8th Edition, Wolfram Research, Champaign, Illinois, 2010.

[34] X. Shan, H. Chen, Lattice Boltzmann model for simulating flows with multiple phases and components, Physical Review E 47 (3) (1993) 1815–1819.

[35] M. Latva-Kokko, D. Rothman, Diffusion properties of gradient-based lattice Boltzmann models of immiscible fluids, Physical Review E 71 (5) (2005) 056702.

[36] S. Chen, G. D. Doolen, Lattice Boltzmann method for fluid flows, Annual review of fluid mechanics 30 (1998) 329–364.

[37] K. Mattila, Implementation techniques for the lattice Boltzmann method, Ph.D. thesis, University of Jyvskyl (2010).

[38] D. Rothman, S. Zaleski, Lattice-Gas Cellular Automata: Simple Models of Complex Hydrodynamics, Aléa-Saclay, Cambridge University Press, 2004.